


Article

Stratosphere–Troposphere Exchange and O₃ Variability in the Lower Stratosphere and Upper Troposphere over the Irene SHADOZ Site, South Africa

Thumeka Mkololo ^{1,2,*}, Nkanyiso Mbatha ³, Venkataraman Sivakumar ¹ , Nelson Bègue ⁴, Gerrie Coetzee ² and Casper Labuschagne ²

¹ School of Chemistry and Physics, University of KwaZulu Natal, Private Bag x 54001, Westville Campus, Durban 4000, South Africa; venkataramans@ukzn.ac.za

² South African Weather Service, Global Atmosphere Watch Station, P.O. Box 320, Stellenbosch 7599, South Africa; gerrie.coetzee@weathersa.co.za (G.C.); casper.labuschagne@weathersa.co.za (C.L.)

³ Department of Geography and Environmental Studies, University of Zululand, KwaDlangezwa 3886, South Africa; mbathanb@unizulu.ac.za

⁴ Laboratoire de l'Atmosphère et des Cyclones, LACy UMR 8105, Université de la Réunion, 97400 Réunion Island, French; nelson.begue@univ-reunion.fr

* Correspondence: thumeka.mkololo@weathersa.co.za; Tel.: +27-(0)-21-888-2487

Received: 17 February 2020; Accepted: 7 May 2020; Published: 3 June 2020



Abstract: This study aims to investigate the Stratosphere–Troposphere Exchange (STE) events and ozone changes over Irene (25.5° S, 28.1° E). Twelve years of ozonesondes data (2000–2007, 2012–2015) from Irene station operating in the framework of the Southern Hemisphere Additional Ozonesondes (SHADOZ) was used to study the troposphere (0–16 km) and stratosphere (17–28 km) ozone (O₃) vertical profiles. Ozone profiles were grouped into three categories (2000–2003, 2004–2007 and 2012–2015) and average composites were calculated for each category. Fifteen O₃ enhancement events were identified over the study period. These events were observed in all seasons (one event in summer, four events in autumn, five events in winter and five events in spring); however, they predominantly occur in winter and spring. The STE events presented here are observed to be influenced by the Southern Hemisphere polar vortex. To strengthen the investigation into STE events, advected potential vorticity maps were used, which were assimilated using Modélisation Isentrope du transport Méso–échelle de l’Ozone Stratosphérique par Advection (MIMOSA) model for the 350 K (~12–13 km) isentropic level. These maps indicated transport of high latitude air masses responsible for the reduction of the O₃ mole fractions at the lower stratosphere over Irene which coincides with the enhancement of ozone in the upper troposphere. In general, the stratosphere is dominated by higher Modern Retrospective Analysis for Research Application (MERRA-2) potential vorticity (PV) values compared to the troposphere. However, during the STE events, higher PV values from the stratosphere were observed to intrude the troposphere. Ozone decline was observed from 12 km to 24 km with the highest decline occurring from 14 km to 18 km. An average decrease of 6.0% and 9.1% was calculated from 12 to 24 km in 2004–2007 and 2012–2015 respectively, when compared with 2000–2003 average composite. The observed decline occurred in the upper troposphere and lower stratosphere with winter and spring showing more decline compared with summer and autumn.

Keywords: ozone enhancement; Irene; ozone decline; potential vorticity; ozonesondes

1. Introduction

The stratosphere and troposphere have different characteristics that are useful in identifying air movement from the stratosphere to the troposphere and vice versa. The stratosphere is characterized by high ozone (O_3) and potential vorticity (PV). On the other hand, the troposphere is characterized by low O_3 and PV. Approximately 90% of O_3 is found in the stratosphere and only 10% in the troposphere. Most of the O_3 in the stratosphere is situated within the O_3 layer [1] where it plays a critical role in shielding the environment and protecting human health from dangerous ultraviolet (UV) rays. The O_3 hole was discovered over Antarctica in late 1980's [2,3] and its dynamics with Ozone Depleting Substances (ODS) are well documented [4–6]. The appearance of O_3 hole was a big concern because of the relationship that increased UV can have on various processes in the lower troposphere. In 1998, the Montreal protocol was successfully implemented to phase out the use of ODS. Subsequently, ozone was expected to increase in the stratosphere after ODS were phased out. Since 1985, a decreasing trend of 30 DU in total column O_3 was reported for stations over the southern mid-latitudes [7]. A positive trend was only observed in the upper stratosphere above 10 hPa [8,9]. A continuous O_3 decline (even though statistically non-significant) was reported in the lower stratosphere from 1998 until present for the stations lying between 60° N and 60° S [10].

Tropospheric O_3 mole fractions are controlled by chemical and physical processes, and its precursors originate from both natural and anthropogenic activities. In the troposphere, O_3 is a secondary pollutant formed through a number of reactions containing nitrogen oxides (NO_x), volatile organic compounds (VOCs), methane (CH_4), and CO in the presence of sunlight [11] or through the transportation of O_3 -rich air from the stratosphere. This process of O_3 movement from the stratosphere to the troposphere and vice versa is known as stratosphere–troposphere O_3 exchange (STE). After the Los Angeles photochemical smog, studies revealed that O_3 can either be transported from the stratosphere or produced from chemical reactions involving O_3 precursors in the troposphere [12]. Stratosphere intrusion (SI) are expected to transport high O_3 and PV to the troposphere. Hence, high O_3 , high PV and dry atmospheric air are used to identify stratosphere intrusion events in the troposphere. The STE plays an important role in the chemical budget of O_3 and water vapour of the upper troposphere and lower stratosphere [13]. Stratospheric Intrusion studies are poorly documented in the Southern Hemisphere; hence, it is challenging to find the threshold that could be used to study these events in the literature. Ozone vertical profiles are useful in identifying and studying STE. A number of studies have been undertaken using Irene ozonesondes data. These studies include: (a) study of O_3 climatology over Irene by Diab et al. [14] using 1990 to 1994 and 1998 to 2004 dataset, (b) satellite validation [15,16] of global transport models, (c) a study on stratospheric profile and water vapour in Southern Hemisphere [17], and (d) the study on the Southern Hemisphere tropopause [18]. In their study, Diab et al. [14] reported O_3 enhancement in Irene above 10 km (upper troposphere) which can be related to STEs during late winter. Similar to this study, they also noted the absence of seasonal consistency in the occurrence of these events at a height above 10 km level. The frequency of occurrence of STEs in the Irene SHADOZ data set has never been studied due to limited data availability and the frequency of the launching of ozonesondes. However, according to Diab et al. [14], the STEs events are dominant in winter and spring in the Irene station. In support to these observations, a study by Poulida et al. [19] also found high O_3 mole fractions in the upper troposphere dominating in winter and spring months.

There are limited studies conducted over Southern Africa on STEs. A recent study on high O_3 events was conducted by Mulumba in Nairobi, Congo Basin and Irene using ozonesondes data [20]. However, the focus was more on Nairobi and Congo Basin and little was done with Irene data. Hence, this study focuses on O_3 data observed from Irene station. It is crucial to investigate O_3 enhancement events in the troposphere and determine if such episodes were related to stratosphere–troposphere exchange. Also, events such as Cut-off lows, Rossby waves, Quasi-Biennial Oscillation (QBO) and El Niño–Southern Oscillation (ENSO) are all factors that could potentially play a critical role in STEs [21,22]. For example, QBO affects the troposphere by direct effect of QBO on the tropical or

subtropical troposphere [23]. A downward movement of easterly winds is more dominant and much stronger compared to westerlies. Easterlies are represented as negative on the QBO index while positive signal represents westerlies. Another way that QBO affects the troposphere is through polar vortex [24–26] processes. Most researchers have defined the polar vortex as a region of high PV. The stratosphere polar vortex develops in autumn when there is no solar heating in polar regions, strengthens in winter and breaks down in spring as sunlight returns to polar regions [27]. The breakdown of stratospheric polar vortex especially plays an important role in O₃ distribution in high latitudes [22]. Several studies have investigated the role of the southern polar vortex with respect to the middle atmosphere of the southern hemisphere [28–30]

A comprehensive study on STEs was recently conducted at three Southern Hemisphere stations (Davis (69° S, 78° E), Macquarie Island (55° S, 159° E) and Melbourne (38° S, 145° E)) by looking at the statistical analysis of STEs and their impact on tropospheric O₃ [31]. This study has coupled observed STEs with meteorological conditions such as low pressure fronts, cutoff low pressure system, indeterminate meteorology and smoke plumes. A total number of 45, 47 and 72 events were detected in Davis, Macquarie and Melbourne stations, respectively, from ozonesondes data. The majority of events were related to low pressure fronts with fire plumes contributing the least.

A number of researchers have investigated O₃ trends in the lower troposphere O₃ [32–36] and only a few studies have conducted trends analysis at different altitudes of troposphere and the lower stratosphere [9,37]. A study by Granados–Munoz and Leblanc [38] investigated tropospheric trends at different altitudes over California using a procedure similar to that described by Cooper et al. [33]. In their study, linear fits of medians, 5th percentiles and 95th percentiles were done using least squares method. Statistical significant negative trends were observed in the lower troposphere (4–7 km) in winter for the medians and 5th percentiles. On the other hand, a positive significant trend of 0.3 ppb/year was reported for the upper troposphere (7 to 10 km) for the period of 2000 to 2015. A non-significant trend was reported for layers closer to the tropopause whilst negative trends were observed in the lower stratosphere (17 to 19 km). A recent study by Ball [9] reported a continuous decrease of O₃ in the lower stratosphere in the region between 60° N and 60° S, while ozone recovery was observed in the upper stratosphere.

The aim of this study is to utilise the available Irene ozonesonde vertical profile to investigate the STE events that are known to lead to SI occurrence. Thus, this study identifies O₃ enhancement events exceeding monthly 90th percentile composite in the upper troposphere, and investigate whether such episodes were due to SI events. Another objective of this study is to investigate O₃ changes in the upper troposphere and lower stratosphere using Irene ozonesondes data and linear regression for medians, 5th percentiles and 95th percentiles.

2. Method and Data

2.1. Ozonesondes

Irene station soundings started in 1998 during the Southern African Fire Atmospheric Research Initiative (SAFARI) campaign in the African region. Currently, the station operates within the framework of the Southern Hemisphere Additional Ozonesondes (SHADOZ). The main aim of the project was to determine O₃ mole fractions in the troposphere and stratosphere, and also to have a full coverage of O₃ measurements over Southern Hemisphere. Since then, balloon launching continued in Irene with ozonesondes launched every second Wednesday of each month circumstances allowing. Ozone vertical profiles are obtained using electrochemical concentration cell (ECC). The heart of the instrument is the electrochemical cell that interfaces with a radiosonde that transmits back data signals to the ground station receiver. The method used by the electrochemical cell to detect O₃ was discussed extensively by Sivakumar et al. [39]. A total number of 250 ozonesondes were launched over the study period. Irene ozonesondes data was retrieved from SHADOZ website [40]. It is important to note that there is a data gap of approximately four years (2008 to September 2012) in the Irene data due to

budget constraints and technical problems with the ground receiver. The program was resumed in 2012 when these issues were resolved.

2.2. MERRA-2 Potential Vorticity

The stratosphere has static stability and is known to contain higher potential vorticity (PV) compared with the troposphere. During the stratosphere intrusion episode, an air mass rich in O₃ and high PV enters the lower stratosphere and upper troposphere. Hence, PV can be used to identify troposphere air mass having a stratosphere origin. The tropopause is defined using a PV value as 2 PVU [39,41]. Therefore, any higher PV events located in the troposphere are associated with stratosphere origin. Other studies, have used PV values of 1.5 PVU as a threshold to identify stratosphere air [42,43]. In this study, a PV value of 2 PVU was used as a threshold for stratospheric air. This study employs PV data from the Modern Retrospective Analysis for Research Application version 2 (MERRA-2) with a spatial resolution of $0.5 \times 0.625^\circ$. MERRA-2 model is an Earth System reanalysis model by National Aeronautics Space Administration (NASA) Global Modeling and Assimilation Office (GMAO). More details about MERRA-2 can be found in the website: <https://gmao.gsfc.nasa.gov/reanalysis/MERRA-2/>. Although the units of PV are $\text{Km}^2 \text{kg}^{-1} \text{s}^{-1}$, PV Units (PVU) (where $1 \text{ PVU} = 1 \times 10^{-6} \text{ Km}^2 \text{kg}^{-1} \text{s}^{-1}$) will be used for convenience in this study. This study used NASA instrument Panoply software (see <https://www.giss.nasa.gov>) to view the vertical slices of PV over Irene [44].

2.3. Data Processing

The ozonesonde data is recorded every two seconds from 1.5 km to approximately 28 km. Ozone averages were calculated from 2 seconds data for each kilometer (km) ascended (e.g., 1 km, 2 km, 3 km to 28 km). As the ozonesonde ascends, pressure, temperature, humidity and O₃ (both ppm and DU units) are also recorded. The current study used the available ozonesondes data to investigate high O₃ events. The ozonesonde data was grouped into months in order to calculate averages, standard deviations, medians, 5th and 95th percentiles from 1 to 28 km. Monthly averaged data was used in conjunction with individual high O₃ event profiles to determine how individual profiles differ from their respective monthly composite profiles. This study defines high O₃ event as the event where O₃ exceeds the monthly 90th and 95th percentile composites. Events exceeding these percentile composites were selected as an observed high O₃ events. However, these events might originate from different sources such as plumes, stratospheric-troposphere exchange (STE) and other man made activities that generate O₃ precursors. Due to this reason, potential vorticity (PV) of 2PV was added as another criteria to identify events of stratospheric origin. PV was used in this study because it is one of the characteristics to differentiate between the stratosphere and troposphere air masses. Monthly 90th and 95th percentile composites were calculated from the available data of all ozonesondes launched during the study period. Any profile exceeding the monthly 90th and 95th percentile composites at a height between 6 and 11 km was considered for further investigation. The main reason to focus between 6 km and 11 km is to eliminate tropospheric pollution and to select events that occurred below the tropopause. Our method differs from previous studies that identified Stratospheric Intrusion (SI) events as an event where O₃ exceeds 80 ppb and then within 3 km above decreases by 20 ppb or more to a value less than 120 ppb [45]. This method was not used because it will miss some of the events observed over Irene due to lower O₃ mole fractions in the Southern Hemisphere. Another study used the 99th percentile as a threshold to study SI O₃ events and their impact on tropospheric ozone [31]. Similar percentile threshold was not applied in this study for similar reason stated above. We attempted to use the 95th percentile as a threshold, however, we missed five events. Consequently, we opted to use 90th percentile as a threshold.

Average O₃ composite profiles were calculated for three categories (2000–2003, 2004–2007 and 2012–2015) using the available ozonesondes data. In the case of annual and seasonal O₃ changes, monthly averaged composites were calculated from the available ozonesondes data. Monthly averaged

composites were used to compensate data gaps that occurred in summer and autumn. Hence, only summer and autumn composites were used to fill 2015 data gaps. This exercise was done to prevent the bias that may be caused by months with data gaps in calculating O_3 changes at different altitudes. Data gaps were covered only for 2015, not for the years where there was no ozonesondes data for the complete year. Annual changes were studied by averaging monthly data into yearly averages at different layers such as 13–15 km, 16–18 km, 19–21 km and 22–24 km. Furthermore, the medians, 5th and 95th percentiles were calculated at each layer. The slope was determined by fitting a linear trend to yearly averaged data plotted on the scatter plot. The standard error corresponding to the slope was calculated at each layer for median values, and both the 5th and 95th percentile. Similar approach was used to calculate seasonal O_3 changes.

3. Results and Discussion

Figure 1 indicates the monthly (a) and yearly (b) ozonesondes data launched from year 2000 to year 2015 at Irene station. Over the study period, a total number of 250 ozonesondes were launched from January 2008 to September 2012 showing a significant data gap. However, 12.4% of the launched ozonesondes did not reach above 28 km. A maximum of 25 ozonesondes were launched in October and November, respectively whilst a total of 12 ozonesondes were launched in January over the study period. On a per annual basis, the highest number (39) of ozonesondes were launched in 2000 while 2015 reflects the lowest number (11) of ozonesondes launched. The discrepancy in the annual number of ozonesondes launched was a factor of budgetary constraints as well as some operational issues encountered. In general, the target for this SHADOZ station is to launch at least two ozonesondes per month, which makes a total of 24 launches per year.

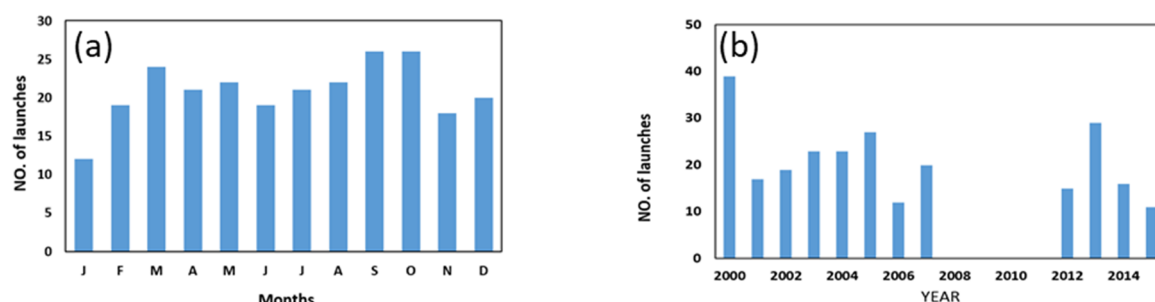


Figure 1. Number of ozonesondes launched at Irene from 2000 to 2015, expressed (a) monthly and (b) annually.

Figure 2. shows O_3 vertical profiles for the troposphere (Figure 2a) and stratosphere (Figure 2b). The data was grouped into three categories namely 2000–2003, 2004–2007, 2012–2015, and the O_3 composite was calculated at kilometre intervals from 1 km to 28 km. The data used in Figure 2 also include 12.4% of ozonesondes that didn't reach 28 km. Therefore, 87.6% of ozonesondes launched over the study period reached 28 km. Three vertical profiles (2000–2003, 2004–2007 and 2012–2015) were compared and the difference between 2000–2003 and 2004–2007 and between 2000–2003 and 2012–2015 was calculated to determine O_3 variation over the years. The percentage decrease for 2004–2007 profiles were calculated from O_3 difference between 2000–2003 and 2004–2007, similarly, the percentage decrease for 2012–2015 was calculated from 2000–2004 and 2012–2015 O_3 difference. A continuous decrease from 2004–2007 and 2012–2015 was apparent at the height between 12 km and 28 km, with highest decrease occurring at a height between 14 km and 18 km. An average decrease of 6.0% and 9.1% was observed at a height between 12 km and 26 km for 2004–2007 and 2012–2015, respectively, when compared to the 2000–2003 period. These results are in agreement with a study by Ball et al. [10] which reported evidence from multiple satellite measurements that ozone in the lower stratosphere between 60° S and 60° N has indeed continued to decline since 1998.

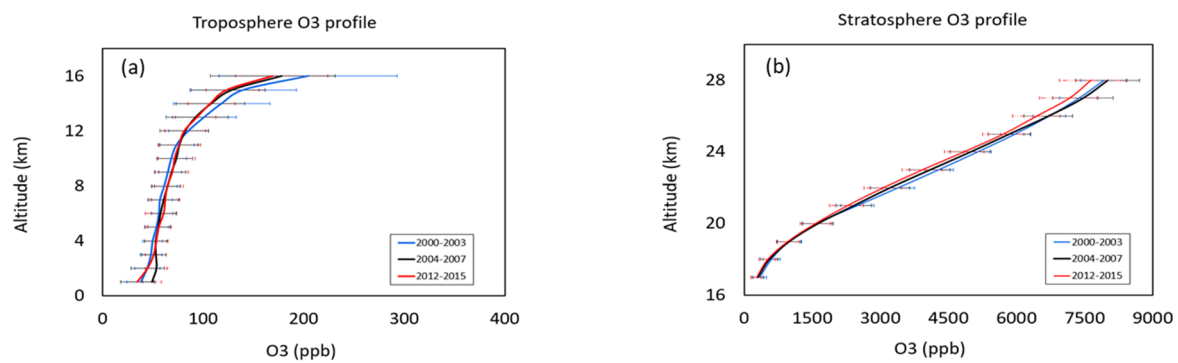


Figure 2. Ozone troposphere (a) and stratosphere (b) profiles. The blue line indicates 2000–2003 averages, black line indicates 2004–2007 averages and red line indicates 2012–2015 averages. The error bars indicate the standard deviation.

Figure 3 shows the O_3 seasonal vertical profiles averages for the troposphere and stratosphere. In the year 2012–2015, summer experienced high O_3 increase from 5 km to 12 km (Figure 3a). On the other hand, 2000–2007 experienced high O_3 mole fractions in the lower troposphere (Figure 3a,c,e,g), with the increase noted up to 8 km during the winter (Figure 3e). On the other hand, O_3 decrease was observed in the upper troposphere and lower stratosphere, with 2012–2015 experiencing lower mole fractions compared to 2004–2007 and 2000–2003 (Figure 3b,d,f,h). In general, a continuous non-consistent O_3 decrease occurred from the upper troposphere (above 16 km) to lower stratosphere (28 km) for all seasons. These results suggest that the observed O_3 decrease in the lower stratosphere is independent of season. Whereas, O_3 increase between 1.5 and 4 km could be related to increase in urban influence boundary layer precursors [46]. Such O_3 precursors could originate from domestic heating and power stations. Maximum standard deviation is observed at altitudes closer to tropopause region. Such increase could be related to STE and other dynamic changes occurring in the tropopause region. This variation was observed to be lesser in summer when compared to other seasons. Sivakumar and Ogunniyi [38] reported similar observations of higher standard deviation closer to the tropopause height.

Tables 1 and 2 summarize statistics of high O_3 events that were obtained by using the 95th and 90th percentile composites and potential vorticity of 2 PVU as thresholds. All episodes that exceeded the monthly 95th percentile composite and 2 PVU were automatically classified as high ozone events (Table 1). However, it was noted that more episodes could be identified when 90th percentile composite is used instead of 95th percentile (Table 2). The monthly average composites, 90th percentile and 95th percentile composites were calculated by using 2000–2015 Irene ozonesondes data. The maximum of the peak was defined as the highest ozone observed from a particular ozone profile at a particular altitude. In this case, it is the maximum of the profile dated on the first column. Delta ozone was defined as the difference between the maximum of a particular event observed at a particular altitude and 90th or 95th percentile composite profile. The altitude of the event was defined as an altitude where maximum values of O_3 occurred. Based on observations indicated in Table 2, it is noted that stratospheric intrusions can reach 7 km altitude over Irene. Similar results of the occurrence of deep intrusions at 7 km altitude were reported at Reunion Island [47]. Clain et al. [47] used different PV thresholds (1.0, 1.5 and 2.0 PVU) on the study of STEs in Reunion Island. Their findings revealed that the number of detected STEs depends on the PV value and duration of back trajectories. About 9.9% STEs were detected using 2 PVU and 2 days back trajectories relative to 28.5% STEs detected using 1 PVU and 10 days back trajectories. In this study, 6.8% STEs were detected using 2 PVU and 90th percentile composite as a threshold. While 4.6% STEs were detected using 2 PVU and 95th percentile composite as a threshold. Figures 4–10b show more events of high PV propagation from the stratosphere to the troposphere. However, in most cases there were some data gaps of ozonesondes.

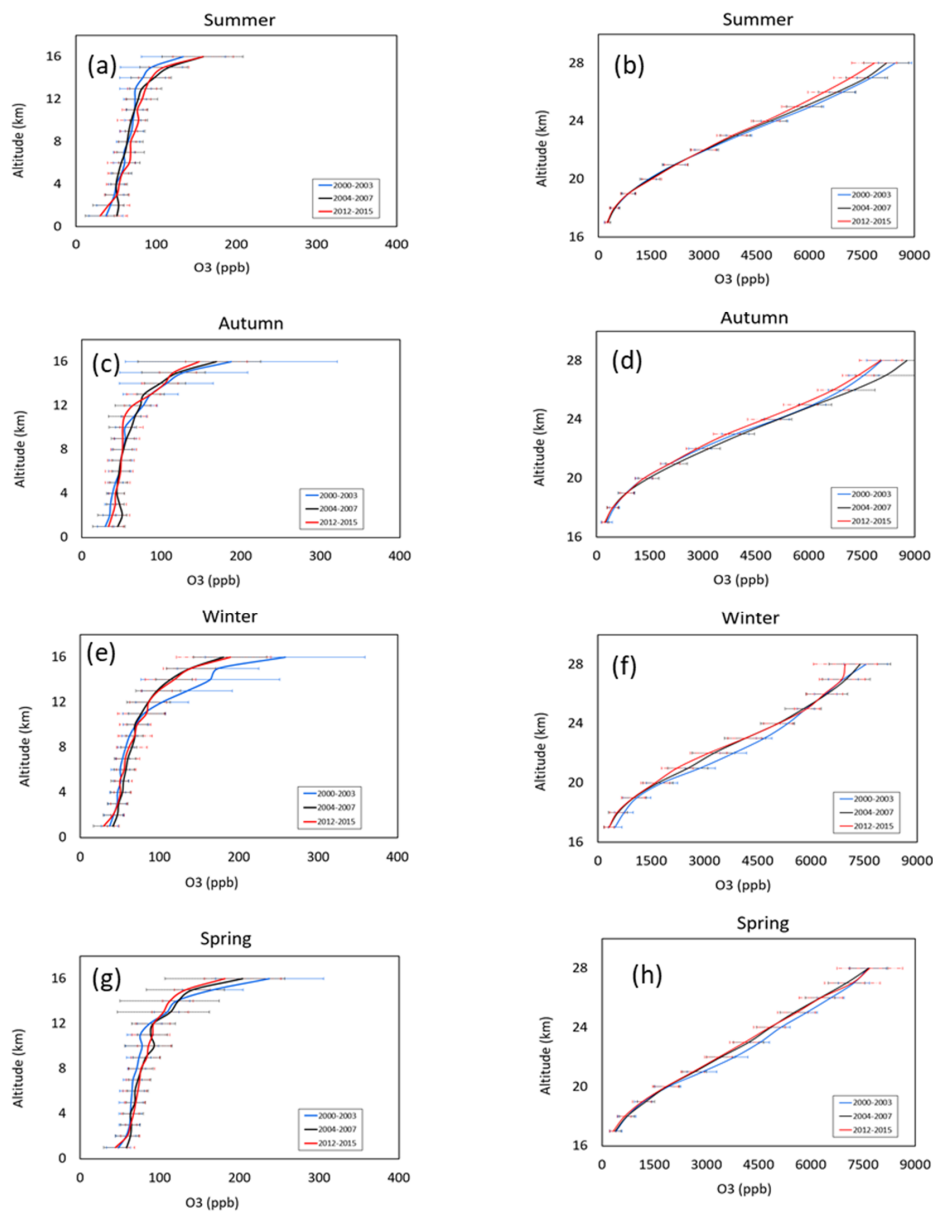


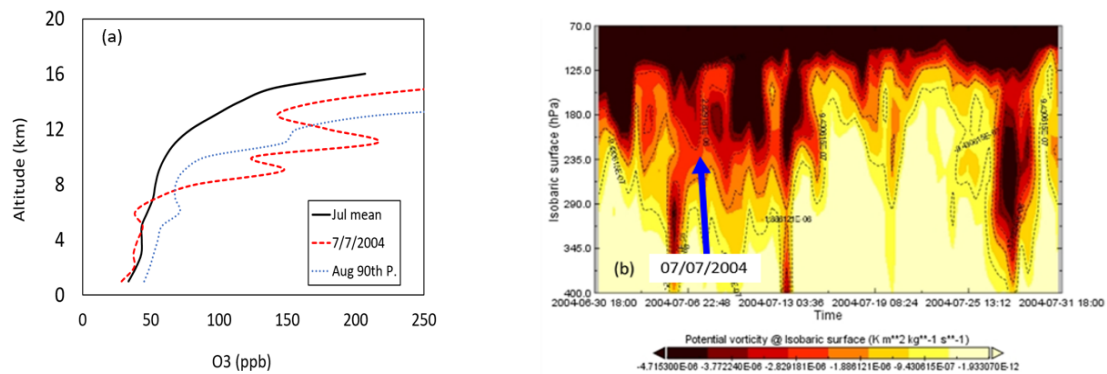
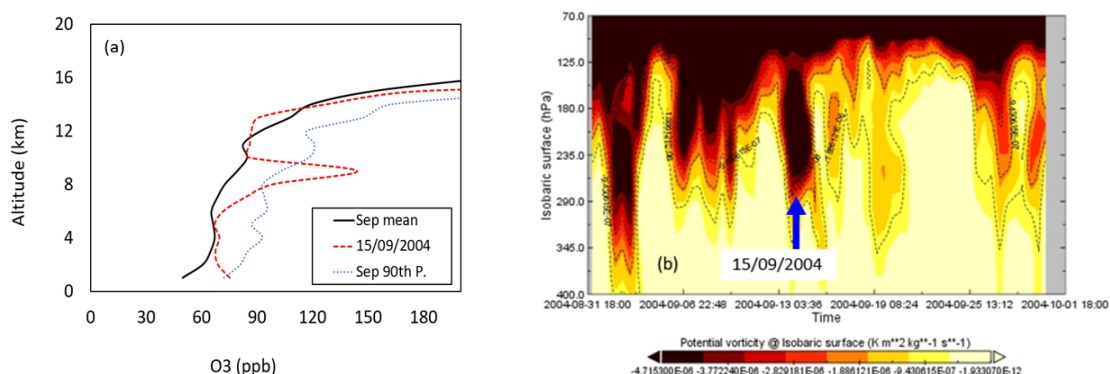
Figure 3. Ozone seasonal profiles for the troposphere (a,c,e,g) and stratosphere (b,d,f,h). Blue line indicates 2000–2003 averages, black line indicates 2004–2007 averages and red line indicates 2012–2015 averages. The error bars indicate the standard deviation.

Table 1. Summary of high ozone (ppb) events statistics using 95th percentile and potential vorticity (2 PVU) as thresholds.

| Date of the Event | Monthly Composite | Monthly 95th Percentile Composite | Maximum Peak of the Event | Delta Ozone | Altitude of the Event |
|-------------------|-------------------|-----------------------------------|---------------------------|--------------|-----------------------|
| 07/08/2002 | 70.00 | 99.00 | 160.50 | 61.50 | 11 |
| 07/07/2004 | 55.68, 67.62 | 74.00, 147.00 | 146.73, 215.51 | 72.73, 68.51 | 9, 11 |
| 15/09/2004 | 79.15 | 103.00 | 144.02 | 41.02 | 9 |
| 26/08/2005 | 71.98 | 99.00 | 171.37 | 72.37 | 11 |
| 12/04/2006 | 58.03 | 110.80 | 120.00 | 9.20 | 11 |
| 08/08/2007 | 58.18 | 99.00 | 105.71 | 6.71 | 9 |
| 10/01/2007 | 74.65 | 93.00 | 110.91 | 17.91 | 11 |
| 31/07/2013 | 60.41 | 90.50 | 121.67 | 31.17 | 10 |
| 16/04/2014 | 50.42 | 72.00 | 81.46 | 9.46 | 9 |
| 25/11/2015 | 91.67 | 134.00 | 162.03 | 28.03 | 10 |

Table 2. Summary of high ozone (ppb) events statistics using 90th percentile and potential vorticity (2 PVU) as thresholds.

| Date of the Event | Monthly Composite | Monthly 90th Percentile Composite | Maximum Peak of the Event | Delta Ozone | Altitude of the Event |
|-------------------|-------------------|-----------------------------------|---------------------------|---------------|-----------------------|
| 07/08/2002 | 70.00 | 96.00 | 160.50 | 64.50 | 11 |
| 27/11/2002 | 87.33 | 99.00 | 117.13 | 18.13 | 9 |
| 03/03/2004 | 64.91 | 82.00 | 87.13 | 5.13 | 9 |
| 07/07/2004 | 55.68, 67.62 | 70.00, 86.00 | 146.73, 215.51 | 76.73, 129.51 | 9, 11 |
| 15/09/2004 | 79.15 | 99.00 | 144.02 | 45.02 | 9 |
| 26/08/2005 | 71.98 | 96.00 | 171.37 | 75.37 | 11 |
| 12/04/2006 | 58.03 | 71.00 | 120.00 | 49.00 | 11 |
| 01/03/2007 | 58.45 | 74.00 | 81.27 | 7.27 | 7 |
| 08/08/2007 | 58.18 | 76.00 | 105.71 | 29.71 | 9 |
| 10/01/2007 | 74.65 | 87.00 | 110.91 | 23.91 | 11 |
| 03/10/2012 | 89.50 | 112.00 | 110.94 | 2.94 | 10 |
| 17/10/2012 | 89.50 | 112.00 | 137.00 | 25.00 | 10 |
| 31/07/2013 | 60.41 | 72.00 | 121.67 | 49.67 | 10 |
| 16/04/2014 | 50.42 | 66.00 | 81.46 | 15.46 | 9 |
| 25/11/2015 | 91.67 | 113.00 | 162.03 | 49.03 | 10 |

**Figure 4.** (a) Ozone troposphere profile over Irene on 07 July 2004. (b) Potential vorticity at Isobaric surface over Irene on July 2004 (from MERRA-2). Solid line in Figure 4a indicates monthly O₃ average composite, broken line indicates O₃ event and dotted line indicate 90th percentile composite. Colours in Figure 4b indicates the level of potential vorticity, black indicates high potential vorticity of more than 3 Km⁻² kg⁻¹s⁻¹ while yellow indicates potential vorticity of less than 2 Km⁻² kg⁻¹s⁻¹. Blue arrow in Figure 4b indicates the event that is associated with O₃ profile in Figure 4a.**Figure 5.** (a) Ozone troposphere profile over Irene on 15 September 2004. (b) Potential vorticity at Isobaric surface over Irene on July 2004 (from MERRA-2). Solid line in Figure 5a indicates monthly O₃ average composite, broken line indicates O₃ event and dotted line indicate 90th percentile composite. Colours in Figure 5b indicates the level of potential vorticity, black indicates high potential vorticity of more than 3 Km⁻² kg⁻¹s⁻¹ while yellow indicates potential vorticity of less than 2 Km⁻² kg⁻¹s⁻¹. Blue arrow in Figure 5b indicates the event that is associated with O₃ profile in Figure 5a.

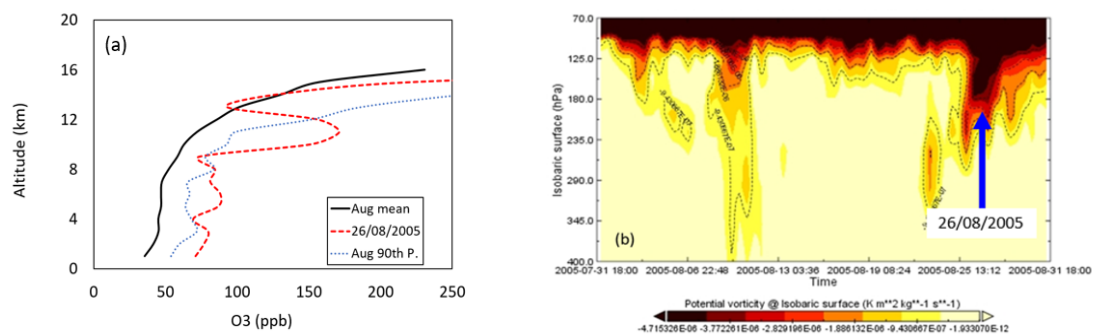


Figure 6. (a) Ozone troposphere profile over Irene on 26 August 2005. (b) Potential vorticity at Isobaric surface over Irene on July 2004 (from MERRA-2). Solid line in Figure 6a indicates monthly O₃ average composite, broken line indicates O₃ event and dotted line indicate 90th percentile composite. Colours in Figure 6b indicates the level of potential vorticity, black indicates high potential vorticity of more than $3 \text{ Km}^{-2} \text{ kg}^{-1} \text{ s}^{-1}$ while yellow indicates potential vorticity of less than $2 \text{ Km}^{-2} \text{ kg}^{-1} \text{ s}^{-1}$. Blue arrow in Figure 6b indicates the event that is associated with O₃ profile in Figure 6a.

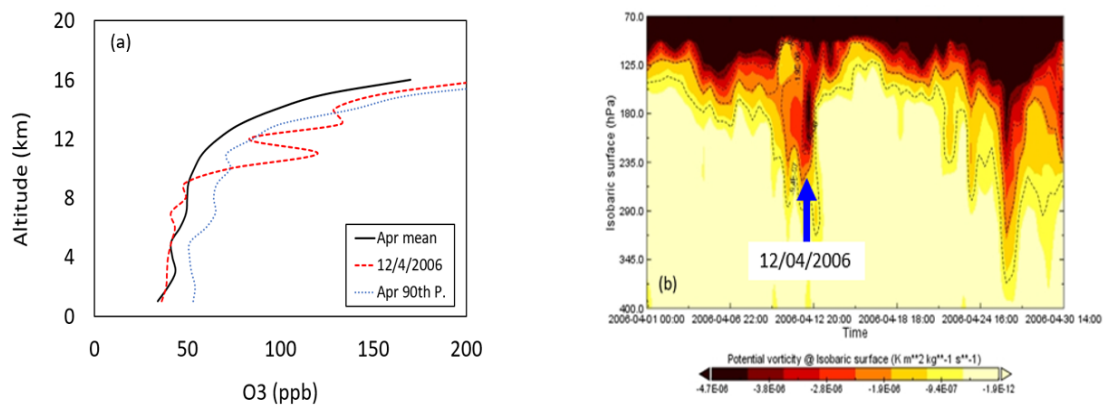


Figure 7. (a) Ozone troposphere profile over Irene on 12 April 2006. (b) Potential vorticity at Isobaric surface over Irene on July 2004 (from MERRA-2). Solid line in Figure 7a indicates monthly O₃ average composite, broken line indicates O₃ event and dotted line indicate 90th percentile composite. Colours in Figure 7b indicates the level of potential vorticity, black indicates high potential vorticity of more than $3 \text{ Km}^{-2} \text{ kg}^{-1} \text{ s}^{-1}$ while yellow indicates potential vorticity of less than $2 \text{ Km}^{-2} \text{ kg}^{-1} \text{ s}^{-1}$. Blue arrow in Figure 7b indicates the event that is associated with O₃ profile in Figure 7a.

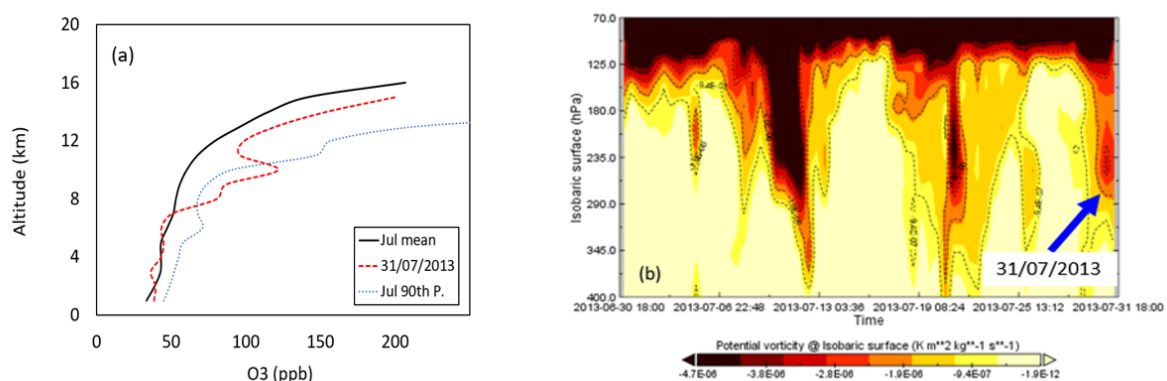


Figure 8. (a) Ozone troposphere profile over Irene on 31 July 2013. (b) Potential vorticity at Isobaric surface over Irene on July 2004 (from MERRA-2). Solid line in Figure 8a indicates monthly O₃ average composite, broken line indicates O₃ event and dotted line indicate 90th percentile composite. Colours in Figure 8b indicates the level of potential vorticity, black indicates high potential vorticity of more than $3 \text{ Km}^{-2} \text{ kg}^{-1} \text{ s}^{-1}$ while yellow indicates potential vorticity of less than $2 \text{ Km}^{-2} \text{ kg}^{-1} \text{ s}^{-1}$. Blue arrow in Figure 8b indicates the event that is associated with O₃ profile in Figure 8a.

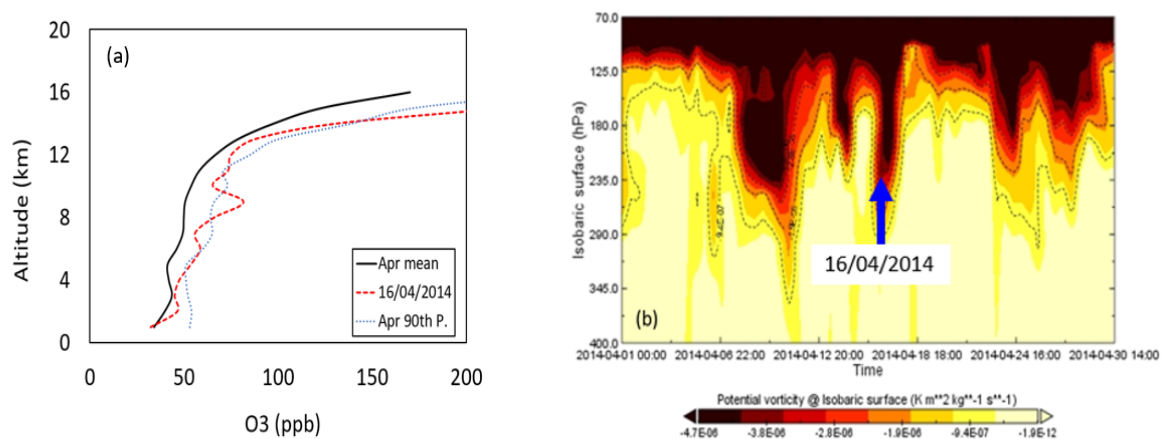


Figure 9. (a) Ozone troposphere profile over Irene on 16 April 2014. (b) Potential vorticity at Isobaric surface over Irene on July 2004 (from MERRA-2). Solid line in Figure 9a indicates monthly O₃ average composite, broken line indicates O₃ event and dotted line indicate 90th percentile composite. Colours in Figure 9b indicates the level of potential vorticity, black indicates high potential vorticity of more than $3 \text{ Km}^{-2} \text{ kg}^{-1} \text{ s}^{-1}$ while yellow indicates potential vorticity of less than $2 \text{ Km}^{-2} \text{ kg}^{-1} \text{ s}^{-1}$. Blue arrow in Figure 9b indicates the event that is associated with O₃ profile in Figure 9a.

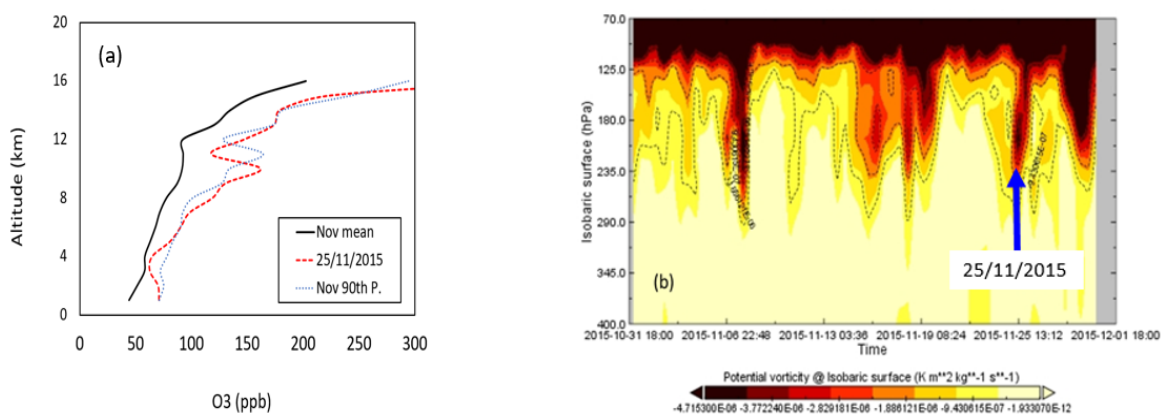


Figure 10. (a) Ozone troposphere profile over Irene on 25 November 2015. (b) Potential vorticity at Isobaric surface over Irene on July 2004 (from MERRA-2). Solid line in Figure 10a indicates monthly O₃ average composite, broken line indicates O₃ event and dotted line indicate 90th percentile composite. Colours in Figure 10b indicates the level of potential vorticity, black indicates high potential vorticity of more than $3 \text{ Km}^{-2} \text{ kg}^{-1} \text{ s}^{-1}$ while yellow indicates potential vorticity of less than $2 \text{ Km}^{-2} \text{ kg}^{-1} \text{ s}^{-1}$. Blue arrow in Figure 10b indicates the event that is associated with O₃ profile in Figure 10a.

3.1. High O₃ Events

In this study, events with high O₃ mole fractions exceeding monthly 90th percentile composites were selected and discussed in terms of PV retrieved using MERRA-2 reanalysis system. As indicated on a PV chart (PV plotted on an isotropic surface) in Figure 4, values outside the contour lines appear relatively low with PV values of about $-1.9 \times 10^{-12} \text{ Km}^{-2} \text{ kg}^{-1} \text{ s}^{-1}$ compared with values inside the contour lines, which have PV values ranging between -4.7×10^{-6} to $1.9 \times 10^{-6} \text{ Km}^{-2} \text{ kg}^{-1} \text{ s}^{-1}$. Higher PV values in the troposphere indicate air mass of stratospheric origin due to increased static stability. PV is generally negative in the Southern Hemisphere (SH) and is usually multiplied by negative one (−1) to appear positive [48,49]. In general, higher values of PV are found in the stratosphere than in the troposphere.

Stratosphere polar vortex forms during autumn in Southern Hemisphere [50]. Moreover, with regards to the geographic position of Irene, this location experiences anticyclonic gyre due to midlatitude westerly waves that occur in autumn and winter [51]. These anticyclonic gyres are responsible for increase in pollutant concentrations for a long period [14]. Two possible stratosphere–troposphere O₃ autumn events (12 April 2006 and 16 April 2014) were selected for discussion.

For the purpose of this study, three possible stratosphere–troposphere O₃ winter events (7 July 2004, 26 August 2005 and 31 July 2013) were selected for discussion. Generally, one may conclude that activities such as anticyclone patterns, domestic usage of biofuels for heating, power generating plants and STEs are the cause of higher O₃ enhancement during this period in Irene [51]. Furthermore, during this season, stratospheric polar vortex starts to be very active in polar region [50].

Also, in this study, two high O₃ events (15 September 2004 and 25 November 2015) were selected in spring and discussed. It is well known that the spring O₃ enhancement events can either be caused by biogenic emissions, biomass burning and lightning production or a combination of them all [11]. However, the occurrence of STEs is dominant in winter and spring over the study area [14], and during this time, the stratospheric polar vortex is more active. According to Clain et al. [47], it is possible that O₃ mole fractions related to stratosphere intrusion can be influenced by climatological O₃ background.

3.2. Case Studies on High Ozone Events

Figures 4a–10a show events that were selected for the case study. These events are part of the fifteen high O₃ events that were identified over the study period. Since these events took place in the month of April, July, August and September, 90th percentile composites for these months were used as thresholds. On these days, high O₃ peaks exceeding the monthly 90th percentile composites were observed between 9 km and 11 km. Figures 4b–10b show MERRA-2 potential vorticity plotted against the isobaric surface between 70 hPa and 400 hPa. These vertical PV slices are for the whole month for the selected events, and averaged to the closest latitude and longitude to Irene SHADOZ site. As indicated on the PV slices, there are several episodes observed in these months where air masses with higher PV of approximately 3.0 PVU propagated from the lower stratosphere (70 hPa) to the upper troposphere (400 hPa). These events are shown as the downward tongues on the PV slices. However, for the purpose of this study, we focus on the time scale closer to the event dates. Blue arrows in PV slices indicate the events that are associated with high O₃ in vertical profiles. As indicated by O₃ vertical profiles, the observed high O₃ events coincides with high PV observed in the higher troposphere. Therefore, it can be reasonably concluded that the observed high O₃ in the upper troposphere could be of stratospheric origin.

3.3. Dynamical Context Using MIMOSA Model

There are several studies that have shown that the dynamics of the Southern Hemisphere polar vortex has an influence in the nearby surrounding structures (upper troposphere and stratosphere) of the Southern Hemisphere [28–30]. A useful method that can assist in profiling the isentropic transport across the dynamical barriers in the stratosphere is the MIMOSA (Modélisation Isentrope du transport Méso-échelle de l’Ozone Stratosphérique par Advection) model. MIMOSA model is a high-resolution advection contour model that is based on Ertel’s potential vorticity which was developed at the Service d’Aéronomie by Hauchecorne et al. [52]. The advection is driven by ECMWF meteorological analyses at a resolution of $0.5^\circ \times 0.5^\circ$. In the case of the PV, its slow adiabatic evolution is taken into account by relaxing the model PV towards the PV calculated from the ECMWF fields with a relaxation time of 10 days. Using this procedure, it is possible to run the model continuously and follow the evolution of PV filaments during several months. This model system enables the investigation of the contribution of the horizontal transport mechanism in the vertical distribution of ozone over high latitudes, mid-latitudes and subtropics. The model gives as an output the advected potential vorticity (APV) with a resolution of $0.3^\circ \times 0.3^\circ$ which is measured in potential vorticity units (PVU) which corresponds to $1 \times 10^{-6} \text{ Km}^{-2} \text{ kg}^{-1} \text{ s}^{-1}$.

In their recent study, Orte et al. [30] successfully showed the influence of the polar vortex over Rio Gallegos, Argentina by using the APV calculated from the MIMOSA high-resolution advection model. Having adopted a similar approach in this study, the influence of the dynamics of the polar vortex over Irene during the days where the STE was observed is also investigated using the APV outputs from the MIMOSA model. The APV maps assimilated using MIMOSA model for the 350 K isentropic level plotted for the 07 July 2004 (a), 15 September 2004 (b), 26 August 2005 (c), 12 April 2006 (d), 30 July 2013 (e), 31 July 2013 (f), 16 April 2014 (g), and 25 November 2015 (h) are shown in Figure 11. The location of Irene is indicated by a black dot in the maps. The slices of APV for 350 K isentropic level which is equivalent to 12–13 km were selected because this is found to be an appropriate pressure level to investigate an STE event.

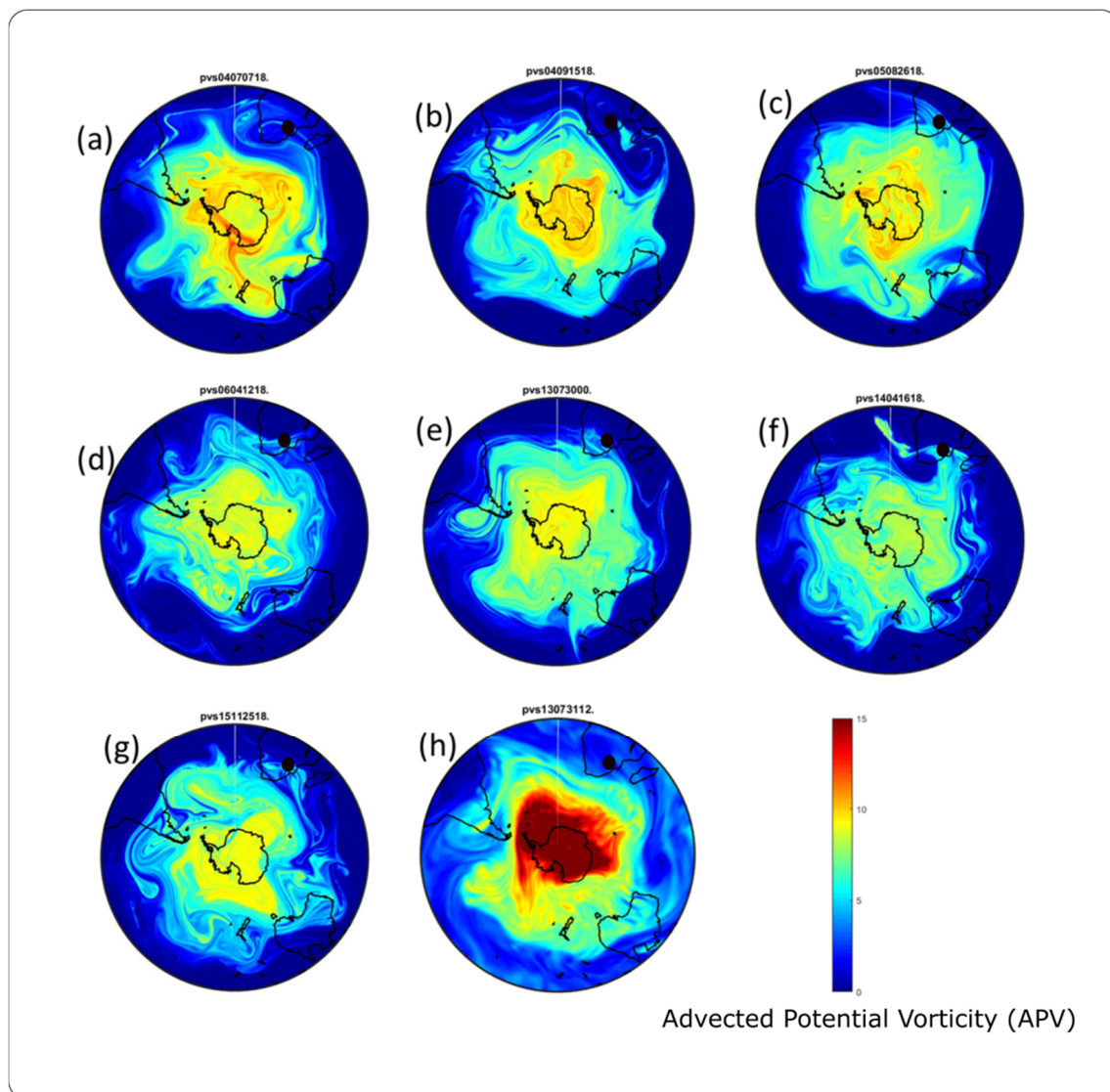


Figure 11. Advected Potential Vorticity (APV) maps assimilated with the MIMOSA model for the 350 K isentropic level (in PVU) and for 07 July 2004 (a), 15 September 2004 (b), 26 August 2005 (c), 12 April 2006 (d), 30 July 2013 (e), 31 July 2013 (f), 16 April 2014 (g), and 25 November 2015 (h). The black dot represents the location of the Irene site.

In general, during all these days which experienced STE process there is obvious passing of APV values with an averaged value of 8 PVU over Irene, South Africa. This is confirmed by blue tongue at the 350 K isentropic level that reflect higher PV values passing over Irene during the days of the STE that were profiled in this study. It can thus be reasoned that this isentropic transport seems to be responsible for the observed reduction of the O₃ mole fractions at the lower stratosphere over Irene which takes place at the same time with the enhancement of ozone in the upper troposphere. The possible dynamical event which is well simulated by the MIMOSA model during the STEs presented here could be that the high APV values are transported from the high latitudes towards the tropics bringing air masses that contain lower ozone concentrations. There is an upward propagation of the middle atmosphere planetary waves in the high and mid-latitudes regions which results to downward propagation around the lower latitudes of the lower stratosphere [28]. The O₃ mole fractions in the lower stratosphere are transported to the upper troposphere, and hence the observed STEs. The influence of the high latitude stratospheric air masses over Irene were also reported on by Semane et al. [28] via their study of the dynamics of the middle atmosphere during the winter of year 2002. Besides, this was a special winter in the southern hemisphere because of the unprecedented year 2002 major stratospheric warming [53,54].

Diab et al. [14] reported a tropopause folding event that occurs during the winter and spring transition period in Irene. The tropopause folding is a good indicator of a STE physical process [14]. Thus, with an improvement of SHADOZ data collection at Irene site since then, it is always important to investigate such a physical process in this study. Figure 12 shows monthly averaged composite of O₃ vertical profiles measured at Irene for the year period from 2000 to 2015. These profiles were plotted for the height region ranging from 1 km to 15 km for January (Jan) to December (Dec). There is a general significant intrusion of higher O₃ mole fractions which are sourced from the stratosphere which is observed in late winter and spring months. In their study, Diab et al. associated this O₃ injection to middle troposphere with westerly winds, which marks the end of maritime season [14]. Also, the subtropical jet was reported to play a role in permitting ozone-rich stratospheric air to penetrate into the troposphere [55]. While most of the free troposphere over Irene was characterised by O₃ mole fraction of approximately 55–60 ppb, the late winter months experience an increase of O₃ concentration to approximately 80 ppb just above the planetary boundary layer. It is also worth noting that the spring season is the period where there are activities such as anthropogenic pollutants sourced from the Congo region and Highveld region biomass burning, and natural activities such as lightning from rainy season and biogenic activities [56]. On the other hand, a similar observation to that which was reported by Diab et al. [14], the tropical tropopause layer (TTL) with O₃ mole fraction ranging between 95 ppb and 100 ppb at a height above 14 km from January to February, while it noticeably declined throughout the year, and approached its minimum altitude of 11 km in October.

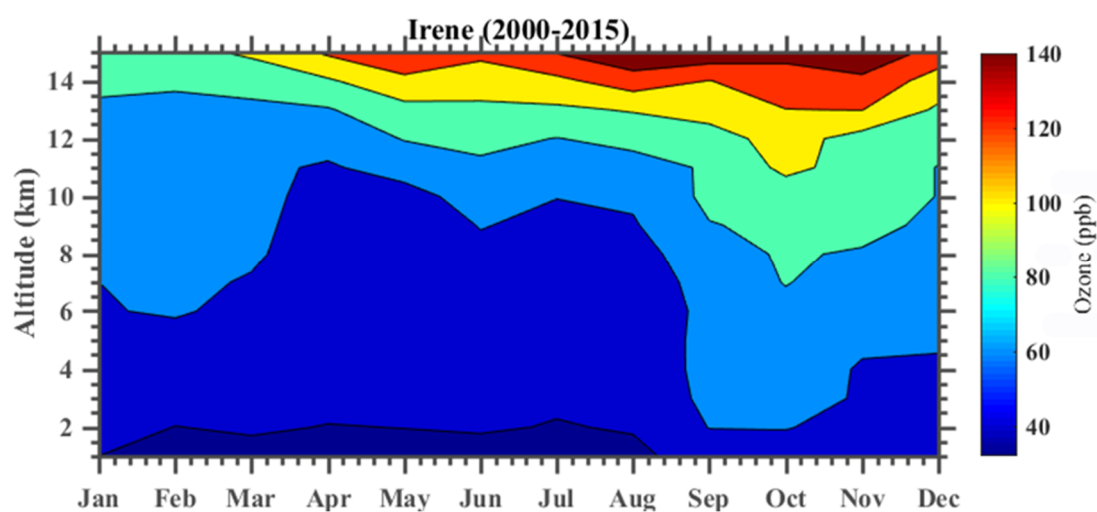


Figure 12. Contour plot of Irene O₃ mole fraction (in ppb) for the period, 2000 to 2015.

3.4. Ozone Decline in Lower Stratosphere

The recovery of O₃ in the upper stratosphere has been well discussed [9,57–61]. However, the investigation of O₃ recovery at different altitude starting from the lower stratosphere upwards still needs attention. This also arise because some recent studies seem to have reported that there may be a continuous decline of O₃ at the lower stratosphere [10,62]. A recent study by Sivakumar and Ogunniyi [38] divided ozonesondes data into two categories, namely tropospheric (0–15 km) and stratospheric region (15–30 km) and reported O₃ maximum occurrence between 22–27 km. Thus, in this study, we also investigate the O₃ decline in the lower stratosphere by using Irene ozonesondes data. Ozone decline is calculated by using medians, 5th and 95th percentiles. Moreover, a composite was calculated at different altitudes (e.g., 13–15 km, 16–18 km and 19–21 km) of the upper troposphere and stratosphere. Rate of change was then calculated by fitting a linear trend on the graphs.

3.4.1. Annual Changes at Different Altitudes

Table 3 summarises the statistics calculated for the medians, 5th and 95th percentiles. Layers corresponding to the upper troposphere (7–9 km) show a positive change of 0.33 ± 0.57 , 0.19 ± 0.56 and 0.38 ± 0.88 ppb/year for the median, 5th and 95th percentiles respectively. Similarly, at 10–12 km height, a positive change of 0.29 ± 0.58 and 0.24 ± 1.25 ppb/year was observed for the median and 95th percentile respectively. In contrast, a negative change of 2.58 ± 3.90 , -0.59 ± 3.17 and -9.63 ± 9.27 ppb/year was observed at 16–18 km for the median, 5th and 95th percentile respectively. Similarly, negative changes were observed at 19–21 and 22–24 km for median, 5th and 95th percentiles. In summary, the results presented here indicate that there are negative changes in the lower stratosphere, while the upper troposphere shows a positive change. Similar observations of O₃ decline in the lower stratosphere were reported by Granados-Munoz and Leblanc [37] when studying tropospheric O₃ seasonal and long-term variability at the JPL–Table Mountain. Furthermore, Ball et al. [10] suggested that lower stratosphere decline contributes to the observed total column O₃ decline. Therefore, the results presented here are consistent with the previous observations reported in literature [10,37].

Table 3. Statistical analysis of ozone at different altitudes.

| Altitude | Median [ppb/year] | 5th Percentile [ppb/year] | 95th Percentile [ppb/year] |
|----------|--------------------|---------------------------|----------------------------|
| 7–9 km | 0.33 ± 0.57 | 0.19 ± 0.56 | 0.38 ± 0.88 |
| 10–12 km | 0.29 ± 0.58 | -0.08 ± 0.78 | 0.24 ± 1.25 |
| 13–15 km | 0.21 ± 1.04 | 0.47 ± 1.13 | -2.38 ± 3.28 |
| 16–18 km | -2.58 ± 3.90 | -0.59 ± 3.17 | -9.63 ± 9.27 |
| 19–21 km | -6.95 ± 13.07 | -7.04 ± 9.83 | -9.46 ± 18.31 |
| 22–24 km | -16.16 ± 21.83 | -21.19 ± 27.39 | -14.81 ± 21.82 |

3.4.2. Seasonal Changes at Different Altitudes

Figure 13 indicates O₃ changes calculated using linear regression at different altitudes during summer, autumn, winter and spring season. And, Table 4(a,b,c,d) provide summery statistics (Median, 5th and 95th percentiles) of these changes. Standard deviation values close to zero indicate O₃ observed over the years was close to the calculated mean. The observations in these tables can be summarised as follows:

7–9 km layer: there was a negative change identified in autumn (-0.11 ± 0.53 ppb/year). While there was a positive change observed in summer (0.53 ± 0.40 ppb/year), winter (0.85 ± 0.72 ppb/year) and spring (0.04 ± 0.57 ppb/year) for the medians. Similarly, there was a positive change observed for the 5th percentiles in summer (0.60 ± 0.58 ppb/year), autumn (0.40 ± 0.34 ppb/year) and winter (0.02 ± 0.17 ppb/year). While spring (-0.02 ± 0.22 ppb/year) showed a negative change. There was a negative change observed in spring (-0.54 ± 1.00 ppb/year), while a positive change was observed in summer (0.23 ± 0.78 ppb/year), autumn (0.68 ± 0.79 ppb/year) and winter (1.14 ± 0.94 ppb/year) for the

95th percentiles. Therefore, it can be concluded that an overall positive change is dominant in this layer for most of the seasons.

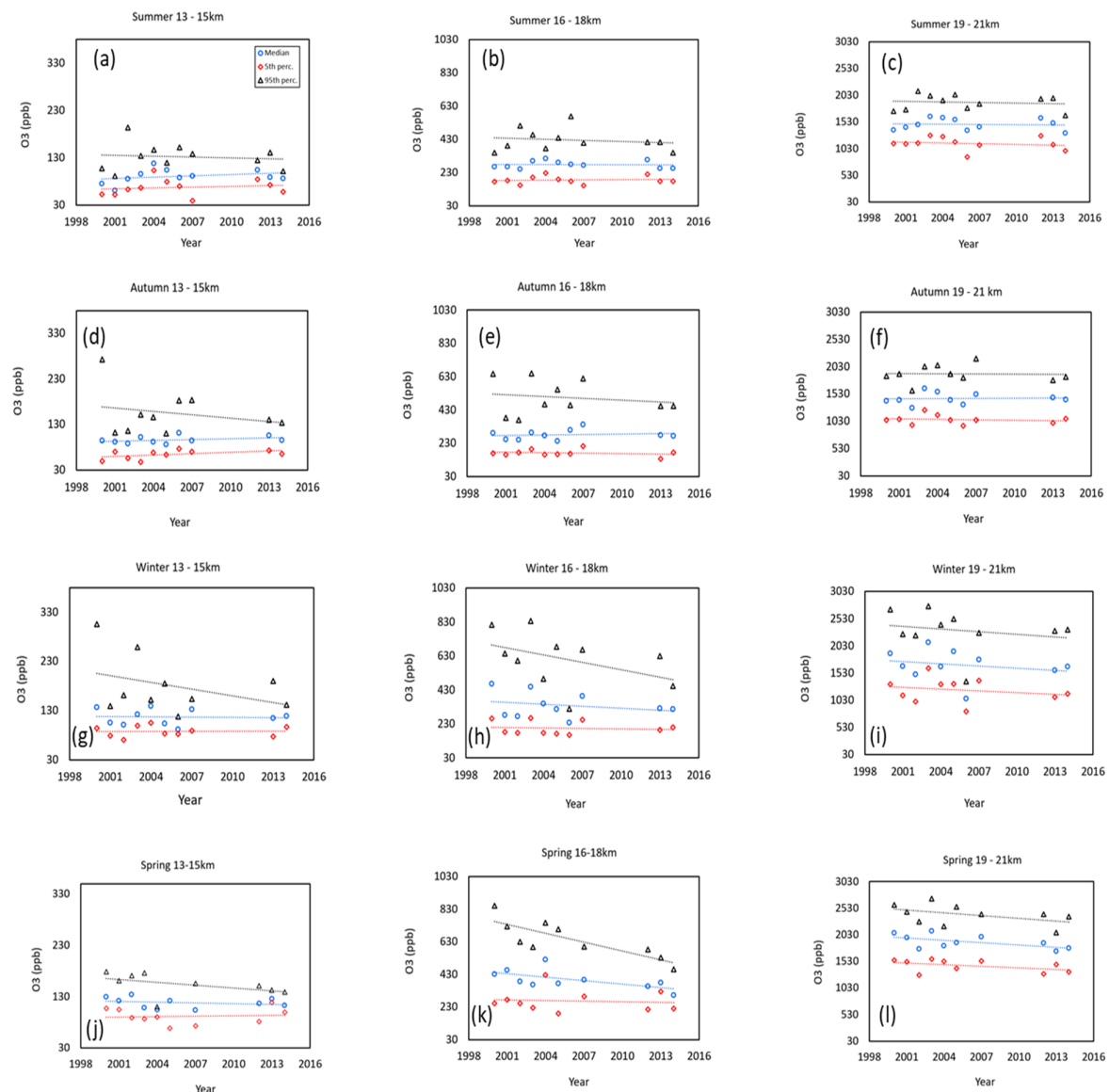


Figure 13. Ozone time series (2000–2015) of the 5th (red), median (blue) and 95th (black) percentile ozone mole fractions at different altitude, (a) summer 13–15 km, (b) summer 16–18 km and (c) summer 19–21 km, (d) autumn 13–15 km, (e) autumn 16–18 km, (f) autumn 19–21 km, (g) winter 13–15 km, (h) winter 16–18 km, (i) winter 19–21 km, (j) spring 13–15 km, (k) spring 16–18 km and (l) spring 19–21 km. Dashed lines represent the linear fit for each time series.

10–12 km layer: there was a negative change observed in autumn for the medians (-0.03 ± 0.81 ppb/year) and for the 5th percentiles in summer (-0.07 ± 0.66 ppb/year), autumn (-0.13 ± 0.61 ppb/year) and winter (-1.00 ± 0.85 ppb/year). Similarly, there was a negative change observed in winter (-0.96 ± 2.03 ppb/year) and spring (-0.36 ± 1.19 ppb/year) for the 95th percentiles. Whilst on the other hand, a positive change was observed in summer (1.09 ± 0.72 ppb/year) and autumn (1.17 ± 1.04 ppb/year) for the 95th percentiles.

13–15 km layer: with the exception of winter (-0.18 ± 1.34 ppb/year) and spring (-0.50 ± 0.88 ppb/year), a positive change was observed in summer (0.91 ± 1.26 ppb/year) and autumn (0.62 ± 0.67 ppb/year) for the medians. Similarly, a positive change was also observed in summer (0.59 ± 1.47 ppb/year), autumn (1.02 ± 0.81 ppb/year), winter (0.03 ± 0.93 ppb/year) and spring (0.24 ± 1.31 ppb/year) for the 5th percentiles. Contrasting with the 10–12 km layer, the 95th percentiles yielded negative change in all of the seasons.

Table 4. Ozone statistical summary at different altitudes and seasons.

| Altitude | Median [ppb/year] | 5th Percentile [ppb/year] | 95th Percentile [ppb/year] |
|---|--------------------|---------------------------|----------------------------|
| (a). Summer (\pm indicates the standard deviation) | | | |
| 7–9 km | 0.53 ± 0.40 | 0.60 ± 0.58 | 0.23 ± 0.78 |
| 10–12 km | 0.48 ± 0.49 | -0.07 ± 0.66 | 1.09 ± 0.72 |
| 13–15 km | 0.91 ± 1.26 | 0.59 ± 1.47 | -0.59 ± 2.36 |
| 16–18 km | -0.28 ± 1.84 | 0.56 ± 1.96 | -2.08 ± 5.58 |
| 19–21 km | -1.28 ± 8.96 | -4.69 ± 10.01 | -3.39 ± 12.09 |
| 22–24 km | -21.78 ± 17.53 | -25.66 ± 29.31 | -18.00 ± 14.98 |
| (b). Autumn (\pm indicates the standard deviation) | | | |
| 7–9 km | -0.11 ± 0.53 | 0.40 ± 0.34 | 0.68 ± 0.79 |
| 10–12 km | -0.03 ± 0.81 | -0.13 ± 0.61 | 1.17 ± 1.04 |
| 13–15 km | 0.62 ± 0.67 | 1.02 ± 0.81 | -2.50 ± 4.07 |
| 16–18 km | 0.93 ± 2.53 | -0.87 ± 1.69 | -3.77 ± 8.74 |
| 19–21 km | 1.40 ± 8.90 | -2.94 ± 1.06 | -0.99 ± 13.61 |
| 22–24 km | -12.54 ± 19.67 | -13.77 ± 20.90 | -13.59 ± 19.54 |
| (c). Winter (\pm indicates the standard deviation) | | | |
| 7–9 km | 0.85 ± 0.72 | 0.06 ± 0.56 | 1.14 ± 0.94 |
| 10–12 km | 0.14 ± 0.61 | -1.00 ± 0.85 | -0.96 ± 2.03 |
| 13–15 km | -0.18 ± 1.34 | 0.03 ± 0.93 | -4.57 ± 4.89 |
| 16–18 km | -3.85 ± 6.26 | -0.88 ± 3.31 | -14.46 ± 13.17 |
| 19–21 km | -13.30 ± 23.48 | -10.60 ± 18.75 | -16.47 ± 31.56 |
| 22–24 km | -10.14 ± 31.64 | -25.50 ± 34.14 | -8.47 ± 33.79 |
| (d). Spring (\pm indicates the standard deviation) | | | |
| 7–9 km | 0.04 ± 0.57 | -0.30 ± 0.76 | -0.54 ± 1.00 |
| 10–12 km | 0.57 ± 0.42 | 0.90 ± 1.00 | -0.36 ± 1.19 |
| 13–15 km | -0.50 ± 0.88 | 0.24 ± 1.31 | -1.85 ± 1.80 |
| 16–18 km | -7.11 ± 4.99 | -1.15 ± 5.73 | -18.19 ± 9.57 |
| 19–21 km | -14.61 ± 10.94 | -9.93 ± 9.50 | -17.00 ± 15.99 |
| 22–24 km | -20.18 ± 18.49 | -19.83 ± 25.19 | -19.19 ± 18.97 |

16–18 km layer: with the exception of autumn (0.93 ± 2.53 ppb/year), negative changes were observed in summer (-0.28 ± 1.84 ppb/year), winter (-3.85 ± 6.26 ppb/year) and spring (-7.11 ± 4.99 ppb/year) for the medians. Similarly, there was a negative change observed in autumn (-0.87 ± 1.69 ppb/year), winter (-0.88 ± 3.31 ppb/year) and spring (-1.15 ± 5.73 ppb/year) for the 5th percentiles except in summer (0.56 ± 1.96 ppb/year). The 95th percentiles again showed negative changes in all of the seasons. Standard deviations of more than 1.5 ppb were observed in all seasons.

19–21 km layer: with the exception of autumn (1.40 ± 8.90 ppb/year), negative changes were observed for the medians in summer (-1.28 ± 8.96 ppb/year), winter (-13.30 ± 23.48 ppb/year) and spring (-14.61 ± 10.94 ppb/year). In addition to this, negative changes were also observed in all seasons for the 5th and 95th percentiles. With the exception of 5th percentiles in autumn, standard deviations in excess of 8.0 ppb were calculated in this layer with more variation observed during winter and spring.

22–24 km layer: There was a negative change observed in all seasons for the medians, 5th and 95th percentiles. A standard deviation of more 14.0 ppb was calculated in this layer with more variation in winter and spring. The observed high standard deviations suggest greater significance of changes within this layer.

4. Summary and Conclusions

This study examined Irene O₃ profile data from 2000–2015 in order to identify high O₃ events and to study O₃ decline at different altitudes of the stratosphere. Monthly 90th percentile composites were used as a threshold to identify high O₃ events. Furthermore, PV charts at isobaric level were used to identify high PV air mass of stratospheric origin (more than 2 PVU). Based on the observations, high O₃ events were found to occur in all seasons. However, they were most prevalent in winter and spring. The results showed that high O₃ of stratospheric origin can propagate down to 7 km over Irene.

However, very few events were found to reach this altitude. The majority of events occurred between 9 km and 10 km from the earth surface. Based on the results obtained from the PV charts, high PV values of approximately 3 PVU were observed over Irene.

Furthermore, O₃ data was grouped into three categories: 2000–2003, 2004–20007 and 2012–2015 to investigate possible long-term changes using monthly 5th percentile composites, monthly 95th percentile composites and monthly median composites. Troposphere and stratosphere O₃ vertical profiles were generated for the three datasets (2000–2003, 2004–20007 and 2012–2015). Based on the vertical profile graphs, it was noted that the maximum standard deviation occurred in altitudes closer to the tropopause (approximately 17 km). This could be related to STE and other dynamic changes occurring in the tropopause region.

The annual changes presented in Table 3 show an O₃ decline at 13–15 km for the 95th percentiles (-2.38 ± 3.28 ppb/year) while median and 5th percentile O₃ decline started at the 16–18 km layer. A maximum decline was observed at 22–24 km for the medians (-16.16 ± 21.83 ppb/year), 5th (-21.19 ± 27.39 ppb/year) and 95th percentile (-14.81 ± 21.82 ppb/year). High O₃ decline was observed at 19–21 km and 22–24 km in all seasons. The 95th percentiles show O₃ decline at 13–15 km. While O₃ decline was observed in winter and spring at 10–12 km layer for medians and 95th percentiles. In conclusion, high O₃ of stratospheric origin can occasionally reach down as low as 7 km above Irene. However, 68.8% of these events were observed within the 9 km to 10 km region.

PV charts proved a very useful tool and showed the propagation of stratospheric air masses to the troposphere as further evidence of stratosphere O₃ intrusion for the selected high O₃ episodes in this study. These observations seem to indicate that STE events which are observed in over Irene are strongly driven by the dynamics of the Southern Hemisphere polar vortex.

O₃ decline was observed mainly in the lower stratosphere (16–28 km). However, it was more dominant in winter and spring, while few events were observed in summer and autumn. Contrary to this, O₃ increase was observed in the lower troposphere. These observations of O₃ increase in the lower troposphere are in line with literature reports and were associated with an increase pollution in the lower troposphere.

Author Contributions: Conceptualization, T.M. and N.M.; methodology, T.M.; validation, T.M.; formal analysis, T.M.; N.M. and N.B.; investigation, T.M. and N.M.; resources, T.M.; writing—original draft preparation, T.M.; writing—review and editing, T.M.; N.M.; V.S.; G.C.; C.L.; visualization, T.M.; N.M.; and V.S. All authors have read and agreed to the published version of the manuscript.

Funding: This research was funded jointly by the CNRS (Centre National de la Recherche Scientifique) and the NRF (National Research Foundation) in the framework of the LIA ARSAIO and by the South Africa/France PROTEA Program (project No 42470VA).

Acknowledgments: We thank South African Weather Service and ECMWF for access to the dataset. Our extended gratitude goes to Hassan Bencherif for his meaningful support. The ozonesonde data used here was obtained from the SHADOZ website <https://tropo.gsfc.nasa.gov/shadoz/>.

Conflicts of Interest: The authors declare no conflict of interest.

References

1. Bekki, S.; Lefevre, F. Stratospheric ozone: History and concepts and interactions with climate. *Eur. Phys. J. Conf.* **2009**, *1*, 113–136. [\[CrossRef\]](#)
2. Farman, J.C.; Gardiner, B.G.; Shanklin, J.D. Large losses of total ozone in Antarctica reveal seasonal CLOX/NOX interaction. *Nature* **1985**, *315*, 207–210. [\[CrossRef\]](#)
3. Morrisette, P.M. The evolution of policy responses to stratospheric ozone depletion. *Nat. Res. J.* **1989**, *29*, 793–820.
4. Rowland, F.S.; Molina, M.J. Chlorofluoromethanes in environment. *Rev. Geophys.* **1975**, *13*, 1–35. [\[CrossRef\]](#)
5. Mäder, J.A.; Staehelin, J.; Peter, T.; Brunner, D.; Rieder, H.E.; Stahel, W.A. Evidence for the effectiveness of the Montreal Protocol to protect the ozone layer. *Atmos. Chem. Phys.* **2010**, *10*, 12161–12171. [\[CrossRef\]](#)
6. Scientific assessment of ozone depletion: 2010. In *Global Ozone Research and Monitoring Project-Report No. 52*; World Meteorological Organization (WMO): Geneva, Switzerland, 2011; p. 516.

7. Bodeker, G.E.; Scott, J.C.; Kresher, K.; McKenzie, R.L. Global Ozone Trends in Potential Vorticity Coordinates Using TOMS and GOMEE Inter-Compared Against the Dobson network. *J. Geophys. Res.* **2001**, *106*, 23029–23042. [[CrossRef](#)]
8. Scientific assessment of ozone depletion (2014). In *Global Ozone Research and Monitoring Project Report*; World Meteorological Organization (WMO): Geneva, Switzerland, 2014; p. 416.
9. Ball, W.T.; Alsing, J.; Mortlock, D.J.; Rozanov, E.V.; Tummon, F.; Haigh, J.D. Reconciling differences in stratospheric ozone composites. *Atmos. Chem. Phys.* **2017**, *17*, 12269–12302. [[CrossRef](#)]
10. Ball, W.T.; Alsing, J.; Mortlock, D.J.; Staehelin, J.; Haigh, J.D.; Peter, T.; Tummon, F.; Stübi, R.; Stenke, A.; Anderson, J.; et al. Evidence for a continuous decline in lower stratospheric ozone offsetting ozone layer recovery. *Atmos. Chem. Phys.* **2018**, *18*, 1379–1394. [[CrossRef](#)]
11. Seinfeld, J.H.; Pandis, S.N. *From Air Pollution to Climate Change*; John Wiley and Sons: New York, NY, USA, 1998; p. 1326.
12. Haagen-Smit, A.J. Chemistry and physiology of Los Angeles smog. *Ind. Eng. Chem.* **1952**, *44*, 1342–1346. [[CrossRef](#)]
13. El Amraoui, L.; Atti'e, J.L.; Semane, N.; Claeyman, M.; Peuch, V.-H.; Warner, J.; Ricaud, P.; Cammas, J.-P.; Piacentini, A.; Josse, B.; et al. Midlatitude stratosphere—Troposphere exchange as diagnosed by MLS O3 and MOPITT CO assimilated fields. *Atmos. Chem. Phys.* **2010**, *10*, 2175–2194. [[CrossRef](#)]
14. Diab, R.D.; Thompson, A.M.; Mari, K.; Ramsay, L.; Coetzee, G.J.R. Tropospheric ozone climatology over Irene, South Africa from 1990 to 1994 and 1998 to 2000. *J. Geophys. Res.* **2004**, *109*, JD00479. [[CrossRef](#)]
15. Ziemke, J.R.; Chandra, S.; Duncan, B.N.; Froidevaux, L.; Bhartia, P.K.; Levelt, P.F.; Waters, J.W. Tropospheric ozone determined from Aura OMI and MLS: Evaluation of measurements and comparison with the Global Modeling Initiative's Chemical Transport Model. *J. Geophys. Res.-Atmos.* **2006**, *111*, D19303. [[CrossRef](#)]
16. Ziemke, J.R.; Chandra, S.; Labow, G.J.; Bhartia, P.K.; Froidevaux, L.; Witte, J.C. A global Climatology of Tropospheric and Stratospheric Ozone Derived from AURA OMI and MLS Measurements. *Atmos. Chem. Phys.* **2011**, *11*, 9237–9251. [[CrossRef](#)]
17. Sivakumar, V.; Bencherif, H.; Begue, N.; Thompson, A.M. Tropopause characteristics and variability from 11 years of SHADOZ Observations in the Southern Tropics and Subtropics. *J. Appl. Meteorol. Clim.* **2011**, *50*, 1403–1416. [[CrossRef](#)]
18. Thompson, A.M.; Miller, S.K.; Tilmes, S.; Kollonige, D.W.; Witte, J.C.; Oltmans, S.J.; Johnson, B.J.; Fujiwara, M.; Schmidlin, F.J.; Coetzee, G.J.R.; et al. Southern Hemisphere Additional Ozonesondes (SHADOZ) ozone climatology (2005–2009): Tropospheric and tropical tropopause layer (TTL) profiles with comparisons to OMI-based ozone products. *J. Geophys. Res.-Atmos.* **2012**, *17*, D23301. [[CrossRef](#)]
19. Poulida, O.; Dickerson, R.R.; Heymsfield, A. Stratosphere—Troposphere exchange in a midlatitude mesoscale con–vective complex. 1. Observations. *J. Geophys. Res.* **1996**, *101*, 6823–6836. [[CrossRef](#)]
20. Mulumba, J.-P.; Sivakumar, V.; Afullo, T.J.O. Modeling Tropospheric ozone climatology over Irene (South Africa) using retrieved remote sensing and ground-based measured data. *J. Geosci. Remote Sens.* **2015**. [[CrossRef](#)]
21. Ndarana, T.; Waugh, D.W. The link between cut-off lows and Rossby wave breaking in the Southern Hemisphere. *Q. J. R. Meteorol. Soc.* **2010**, *136*, 869–885. [[CrossRef](#)]
22. Sun, L.; Chen, G.; Robinson, W.A. The Role of Stratospheric Polar Vortex Breakdown in Southern Hemisphere Climate Trends. *BAMS Meteorol. Soc.* **2014**. [[CrossRef](#)]
23. Garfinkel, I.; Hartmann, D.L. The influence of the quasi-biennial oscillation on the troposphere in winter in a Hierarchy of Models. Part 1: Simplified dry GCMs. *AMS Meteorol. Soc.* **2011**. [[CrossRef](#)]
24. Holton, J.R.; Tan, H.C. The influence of the equatorial quasi-biennial oscillation on the global circulation at 50 mb. *J. Atmos. Sci.* **1980**, *37*, 2200–2208. [[CrossRef](#)]
25. Hamilton, K. Effects of an imposed quasi-biennial oscillation in a comprehensive troposphere—Stratosphere—Mesosphere general circulation model. *J. Atmos. Sci.* **1998**, *55*, 2393–2418. [[CrossRef](#)]
26. Baldwin, M.P.; Dunkerton, T.J. Stratospheric harbingers of anomalous weather regimes. *Science* **2001**, *294*, 581–584. [[CrossRef](#)] [[PubMed](#)]
27. Waugh, D.W.; Polvani, L.M. Climatology of intrusions into the tropical upper troposphere. *Geophys. Res. Lett.* **2000**, *27*, 3857–3860. [[CrossRef](#)]

28. Semane, N.; Bencherif, H.; Morel, B.; Hauchecorne, A.; Diab, R.D. An unusual stratospheric ozone decrease in the Southern Hemisphere subtropics linked to isentropic air-mass transport as observed over Irene (25.5 S, 28.1 E) in mid-May 2002. *Atmos. Chem. Phys.* **2006**, *6*, 1927–1936. [[CrossRef](#)]
29. Bencherif, H.; Amraoui, L.E.; Kirgis, G.; Leclair De Bellevue, J.; Hauchecorne, A.; Mzé, N.; Portafaix, T.; Pazmino, A.; Goutail, F. Analysis of a rapid increase of stratospheric ozone during late austral summer 2008 over Kerguelen (49.4 S, 70.3 E). *Atmos. Chem. Phys.* **2011**, *11*, 363–373. [[CrossRef](#)]
30. Orte, P.F.; Wolfram, E.; Salvador, J.; Mizuno, A.; Bègue, N.; Bencherif, H.; Bali, J.L.; d’Elia, R.; Pazmino, A.; Godin-Beekmann, S.; et al. Analysis of a southern sub-polar short-term ozone variation event using a millimetre-wave radiometer. *Ann. Geophys.* **2019**, *37*, 613–629. [[CrossRef](#)]
31. Greenslade, J.W.; Alexander, S.P.; Schofield, R.; Fisher, J.A.; Klekociuk, A.K. Stratospheric ozone intrusion and their impacts on tropospheric ozone. *Atmos. Chem. Phys.* **2017**. [[CrossRef](#)]
32. Helmig, D.; Oltmans, S.J.; Carlson, D.; Lamarque, J.-F.; Jones, A.; Labuschagne, C.; Anlauf, K.; Hayden, K. A review of surface ozone in the polar regions. *Atmos. Environ.* **2007**, *41*, 5138–5161. [[CrossRef](#)]
33. Cooper, O.R.; Parrish, D.D.; Ziemke, J.; Balashov, N.V.M.; Cupeiro, M.; Galbally, I.E.; Gilge, S.; Horowitz, L.; Jensen, N.R.; Lamarque, J.-F.; et al. Global distribution and trends of tropospheric ozone: An observation-based review. *Elem.: Sci. Anthr.* **2014**, *2*. [[CrossRef](#)]
34. Oltmans, S.J.; Lefohn, A.S.; Shadwick, D.; Harris, J.M.; Scheel, H.E.; Galbally, I.; Tarasick, D.W.; Johnson, B.J.; Brunke, E.-G.; Claude, H.; et al. Recent tropospheric ozone changes—A pattern dominated by slow or no growth. *Atmos. Environ.* **2013**, *67*, 331–351. [[CrossRef](#)]
35. Lin, M.; Horowitz, L.W.; Cooper, O.R.; Tarasick, D.; Conley, S.; Iraci, L.T.; Johnson, B.; Leblanc, T.; Petropavlovskikh, I.; Yates, E.L. Revisiting the evidence of increasing springtime ozone mixing ratios in the free troposphere over western North America. *Geophys. Res. Lett.* **2015**, 8719–8728. [[CrossRef](#)]
36. Xu, W.; Lin, W.; Xu, X.; Tang, J.; Huang, J.; Wu, H.; Zhang, X. Long-term trends of surface ozone and its influencing factors at the Mt Waliguan GAW station, China—Part 1: Overall trends and characteristics. *Atmos. Chem. Phys.* **2016**, *16*, 6191–6205. [[CrossRef](#)]
37. Granados-Muñoz, M.J.; Leblanc, T. Tropospheric ozone seasonal and long-term variability as seen by LIDAR and surface measurements at the JPL–Table Mountain Facility, California. *Atmos. Chem. Phys.* **2016**, *16*, 9299–9319. [[CrossRef](#)]
38. Sivakumar, V.; Ogunniyi, J. Ozone climatology and variability over Irene, South Africa determined by ground based and satellite observations. Part 1: Vertical variations in the troposphere and stratosphere. *Atmosfera* **2017**, *30*, 337–353. [[CrossRef](#)]
39. Holton, J.R.; Haynes, P.H.; McIntyre, M.E.; Douglass, R.A.; Roodand, R.B.; Pfister, L. Stratosphere—Troposphere exchange. *Rev. Geophys.* **1995**, *33*, 403–439. [[CrossRef](#)]
40. National Aeronautics and Space Administration Goddard Space Flight Center. Available online: <https://tropo.gsfc.nasa.gov/shadoz/> (accessed on 20 April 2016).
41. Newell, R.E.; Browell, E.V.; Davis, D.D.; Liu, S.C. Western Pacific tropospheric ozone and potential vorticity: Implications for Asian pollution. *Geophys. Res. Lett.* **1997**, *24*, 2733–2736. [[CrossRef](#)]
42. World Meteorological Organization (WMO). *Atmospheric Ozone 1985, Vol. I*; World Meteorological Organization: Geneva, Switzerland, 1986; p. 478.
43. Shapiro, M.A. Turbulent mixing within tropopause folds as a mechanism for the exchange of chemical constituents between the stratosphere and the troposphere. *J. Atmos. Sci.* **1980**, *37*, 994–1004. [[CrossRef](#)]
44. National Aeronautics and Space Administration Goddard Institute for Space Studies Website. Available online: <https://www.giss.nasa.gov/tools/panoply> (accessed on 22 November 2018).
45. Tang, Q.; Prather, M.J. Correlating tropospheric column ozone with tropopause folds: The Aura-OMI satellite data. *Atmos. Chem. Phys.* **2010**, *10*, 9681–9688. [[CrossRef](#)]
46. Thompson, A.M.; Balashov, J.C.; Coetzee, J.R.C.; Thouret, V.; Posny, F. Tropospheric ozone increases over the southern Africa region: Bellwether for rapid growth in Southern Hemisphere pollution? *Atmos. Chem. Phys.* **2014**, *14*, 9855–9869. [[CrossRef](#)]
47. Clain, G.; Baray, J.L.; Delmas, R.; Keckhut, P.; Cammas, J.P. A lagrangian approach to analyse the tropospheric ozone climatology in the tropics: Climatology of stratosphere-troposphere exchange at Reunion Island. *Atmos. Environ.* **2010**, *44*, 968–975. [[CrossRef](#)]
48. Stan, C.; Randall, D.A. Potential vorticity as Meridional coordinate. *BAM Meteorol. Soc.* **2007**, *64*, 23029–23042.

49. Hoang, L.P.; Reeder, M.J.; Berry, G.J.; Schwendike, J. Coherent Potential Vorticity Maxima and Their Relationship to Extreme Summer Rainfall in the Australian and North African Tropics. *J. South. Hemisph. Earth* **2016**, *66*, 424–441. [CrossRef]
50. Waugh, D.W.; Polvani, L.M. *Stratospheric Polar Vortices, in the Stratosphere: Dynamics, Transport, and Chemistry*; Polvani, L.M., Sobel, A.H., Waugh, D.W., Eds.; AGU: Washington, DC, USA, 2013; Volume 190, pp. 43–57.
51. Tyson, P.D.; Preston-Whyte, R.A. *The Weather and Climate of Southern Africa*; Oxford Univ. Press: New York, NY, USA, 2000.
52. Hauchecorne, A.; Godin, S.; Marchand, M.; Heese, B.; Souprayan, C. Quantification of the transport of chemical constituents from the polar vortex to midlatitudes in the lower stratosphere using the high-resolution advection model MIMOSA and effective diffusivity. *J. Geophys. Res.: Atmos.* **2002**, *107*, SOL-32. [CrossRef]
53. Dowdy, A.J.; Vincent, R.A.; Murphy, D.J.; Tsutsumi, M.; Riggan, D.M.; Jarvis, M.J. The large-scale dynamics of the mesosphere—lower thermosphere during the Southern Hemisphere stratospheric warming of 2002. *Geophys. Res. Lett.* **2004**, *31*. [CrossRef]
54. Mbatha, N.; Sivakumar, V.; Malinga, S.B.; Bencherif, H.; Pillay, S.R. Study on the impact of sudden stratosphere warming in the upper mesosphere-lower thermosphere regions using satellite and HF radar measurements. *Atmos. Chem. Phys.* **2010**, *10*, 3397–3404. [CrossRef]
55. Baray, J.L.; Ancellet, G.; Taupin, F.G.; Bessafi, M.; Baldy, S.; Keckhut, P. Subtropical tropopause break as a possible stratospheric source of ozone in the tropical troposphere. *J. Atmos. Sol. Terr. Phys.* **1998**, *60*, 27–36. [CrossRef]
56. Thompson, A.M.; Witte, J.C.; Freiman, M.T.; Phahlane, N.A.; Coetzee, G.J.R. Lusaka, Zambia, during SAFARI-2000: Convergence of local and imported ozone pollution. *Geophys. Res. Lett.* **2002**, *29*. [CrossRef]
57. Bourassa, A.E.; Roth, C.Z.; Zawada, D.J.; Rieger, L.A.; McLinden, C.A.; Degenstein, D.A. Drift corrected Odin-OSIRIS ozone product: Algorithm and updated stratospheric ozone trends. *Atmos. Meas. Tech. Discuss.* **2017**. [CrossRef]
58. Sofieva, V.; Kyrölä, E.; Laine, M.; Tamminen, J.; Degenstein, D.; Bourassa, A.; Roth, C.; Zawada, D.; Weber, M.; Rozanov, A.; et al. Merged SAGE II, Ozone_cci and OMPS ozone profiles dataset and evaluation of ozone trends in the stratosphere. *Atmos. Chem. Phys. Discuss.* **2017**. [CrossRef]
59. Steinbrecht, W.; Froidevaux, L.; Fuller, R.; Wang, R.; Anderson, J.; Roth, C.; Bourassa, A.E.; Degenstein, D.A.; Damadeo, R.; Zawodny, J.M.; et al. An update on ozone profile trends for the period 2000 to 2016. *Atmos. Chem. Phys. Discuss.* **2017**, 1–24. [CrossRef]
60. WMO: Scientific assessment of ozone depletion: 2018. In *Global Ozone Research and Monitoring Project-Report*; World Meteorological Organization: Geneva, Switzerland, 2018; p. 588.
61. Petropavlovskikh, I.; Godin-Beekmann, S.; Hubert, D.; Damadeo, R.; Hassler, B.; Sofieva, V. SPARC/IO3C/GAW, 2019: SPARC/IO3C/GAW Report on Long-Term Ozone Trends and Uncertainties in the Stratosphere. Available online: <https://www.sparc-climate.org/publications/sparc-reports/sparc-report-no-9/> (accessed on 16 May 2019).
62. Wargan, K.; Orbe, C.; Pawson, S.; Ziemke, J.R.; Oman, L.D.; Olsen, M.A.; Coy, L.; Knowland, E.K. Recent decline in extratropical lower stratospheric ozone attributed to circulation changes. *Geophys. Res. Lett.* **2018**, *45*. [CrossRef]

